



ACCESS
Arctic Climate Change
Economy and Society



Project no. 265863

ACCESS
Arctic Climate Change, Economy and Society

Instrument: Collaborative Project

Thematic Priority: Ocean.2010-1 "Quantification of climate change impacts on economic sectors in the Arctic"

**D1.51 – Results of Arctic ocean-sea ice downscaling runs
validated and documented**

Due date of deliverable: **30/04/2014**

Actual submission date: **05/12/2014**

Start date of project: **March 1st, 2011**

Duration: **48 months**

Organisation name of lead contractor for this deliverable: **AWI**

Project co-funded by the European Commission within the Seventh Framework Programme (2007-2013)		
Dissemination Level		
PU	Public	X
PP	Restricted to other programme participants (including the Commission Services)	
RE	Restricted to a group specified by the consortium (including the Commission Services)	
CO	Confidential, only for members of the consortium (including the Commission Services)	

D1.51 Results of Arctic ocean-sea ice downscaling runs validated and documented

Authors: Kathrin Riemann-Campe, Michael Karcher, Frank Kauker, Rüdiger Gerdes

Content:

1. Introduction	2
2. The downscaling experiment.....	3
2.1. Choosing one CMIP5 model for the downscaling experiment	3
2.2. The MPI-ESM-LR and emission scenarios	5
2.3. The MITgcm	6
3. Validation of the downscaling simulations.....	7
3.1. Sea ice area: comparison with OSI SAF data and PIOMAS.....	7
3.2. Sea ice volume: comparison with PIOMAS	8
3.3. Sea ice thickness: comparison with ICESat and PIOMAS.....	9
4. Development of Arctic sea ice until 2040 – the downscaling results	11
4.1. Development of sic and sit in March and September	11
4.2. Development of 'low ice condition' days	12
4.3. Changes along a Northeast Passage	15
5. Summary and Conclusions	17

1. Introduction

Global-coupled models are widely used to project future development of climate and its components in the decades ahead, e.g. Arctic sea-ice area and thickness. For the most recent Intergovernmental Panel on Climate Change Assessment Report No. 5 (IPCC-AR5) more than 30 global-coupled climate models carried out standardised experiments for present conditions and four greenhouse-gas emission scenarios to assess the possible range of climate change in the future. These models are part of the so-called Coupled Model Inter-comparison Project phase 5 (CMIP5) established by the World Climate Research Programme (WCRP) [Taylor *et al.*, 2012]. However, not all of these models are able to represent the past and present sea-ice conditions equally well. There are several reasons: one of them being that the winter sea-ice extent is strongly linked to the position of the North Atlantic current in the respective ocean part of the model. Many models have difficulties to simulate the correct position of this warm water current entering the Arctic and thus fail to simulate the sea-ice extent well in this respect.

Several studies have analysed the Arctic sea-ice distributions in CMIP5 models, including Stroeve *et al.* [2012], Wang and Overland [2012], and Massonnet *et al.* [2012] and identified individual models, which simulate the distribution of sea-ice better than others. Depending on the analysis method and the respective criteria, the list of the “better” models varies. Since in ACCESS we are interested in the Arctic as whole as well as specific sub-regions, we performed our own analysis of the CMIP5 models with a focus on these sub-regions. According to ACCESS partners dealing with resource extraction (WP 4), regions with potential for oil and gas exploitation are of special interest, namely the southern and northern Barents Sea (Fig. 1 region EBB2, EBB3), parts of the Kara Sea (Fig. 1 region WSB2) and off Greenland’s west coast (Fig. 1 region WGEC2). Furthermore, we focus on coastal regions along the Northern Sea Routes, which are relevant for shipping activities in the Arctic, a topic dealt with in the marine transportation and tourism work package (WP2).

To find out which CMIP5 models are performing better in the chosen regions as well as in the entire Arctic, we compare the mean seasonal cycle of monthly mean sea-ice concentration from the model experiments covering the 20th century with those derived from two different satellite products covering two time periods: OSISAF 1979-2005 and SSM/I 1992-2005. The CMIP5 model, which is found to be the best model with respect to observed Arctic sea ice concentration is subsequently applied in a downscaling experiment to benefit from a higher resolution. Technically we downscale the global coupled climate model simulation by forcing a regional couple ocean-sea ice model with atmospheric variables from the CMIP5 model. The regional model is deemed to produce a ‘better’ result for the sea ice distribution because of a better representation of oceanic and sea-ice processes. For the ACCESS project we use a version of the MITgcm tailored for the Arctic and Subarctic region. The representation of oceanic and sea-ice processes, which are influenced by details of the bottom topography and coastline, is improved compared to the coarser climate models.

2. The downscaling experiment

2.1. Choosing one CMIP5 model for the downscaling experiment

To determine which CMIP5 models are doing well in the above-mentioned regions, we compare the mean simulated seasonal cycle of monthly mean sea ice concentration (sic) from the historical CMIP5 experiment (1850-2005) with those from Satellite derived sea ice concentrations for the available period of observation (Fig. 2). For this purpose the more than 30 CMIP5 models were interpolated to a common grid of 0.25° resolution. For each ensemble member of the respective CMIP5 model we then compute the misfit of the simulated mean seasonal cycle of the sic to observed sic from two passive microwave satellite data

1. SSMR and SSM/I sea-ice concentration from the EUMETSAT Ocean and Sea Ice Satellite Application Facility (OSI SAF; Global sea ice concentration reprocessing dataset 1978-2009 (v1.1, 2011); Norwegian and Danish Meteorological Institutes. Available from <http://osisaf.met.no>), data from 1979-2005 are used here.
2. SSM/IS and SSM/I sea-ice concentration from the Centre de Recherche et d'Exploitation Satellitaire (CERSAT), at IFREMER, Plouzan   (France) covering 1991-present. Available from <ftp://ftp.ifremer.fr/ifremer/cersat/products/gridded/psi-concentration/data/arctic/> . Data from 1992-2005 are used here.

The uncertainty of satellite products is high for sea ice with low concentration. Therefore, typically data with sic < 15 % are not used for analysis. We follow this procedure here, too. Furthermore, the uncertainty of satellite products varies with the season. In general, the uncertainty is four times larger in summer (~20 %) than in winter (~5 %). Therefore, the misfit is weighted with a seasonal function acknowledging this variance of uncertainty. The misfit is computed using the following equation:

$$\text{misfit} = \sum \left[\frac{(\text{sic}_{\text{model}} - \text{sic}_{\text{satellite}})^2}{\text{weights}} \right] \text{ with weights} = (1, 1, 1, 1, 1, 1, 2, 4, 2, 1, 1, 1).$$

The computation of the misfit is repeated for each grid box of the whole Arctic with the two different satellite derived sea ice datasets. To summarize the results, the misfit is integrated over each region, respectively the whole Arctic and the mean over all ensemble members of each model is computed. The normalized mean misfit of all models is shown in table 1, where 1 means the simulated sic is closest to observations. The ranking of the models varies considerably depending on the observational datasets and the region analysed (Tab. 1). However, the MPI-ESM-LR model consistently shows the best results in all analyses.

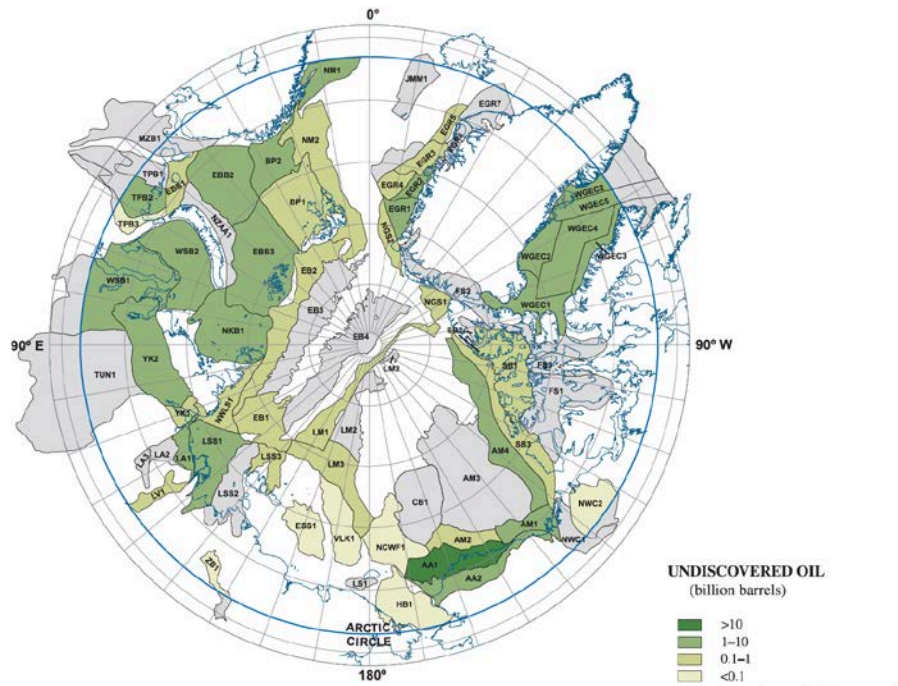


Figure 1: Map from the U.S. Geological Survey showing regions of undiscovered oil. Map is published in *Gautier et al.* [2009].

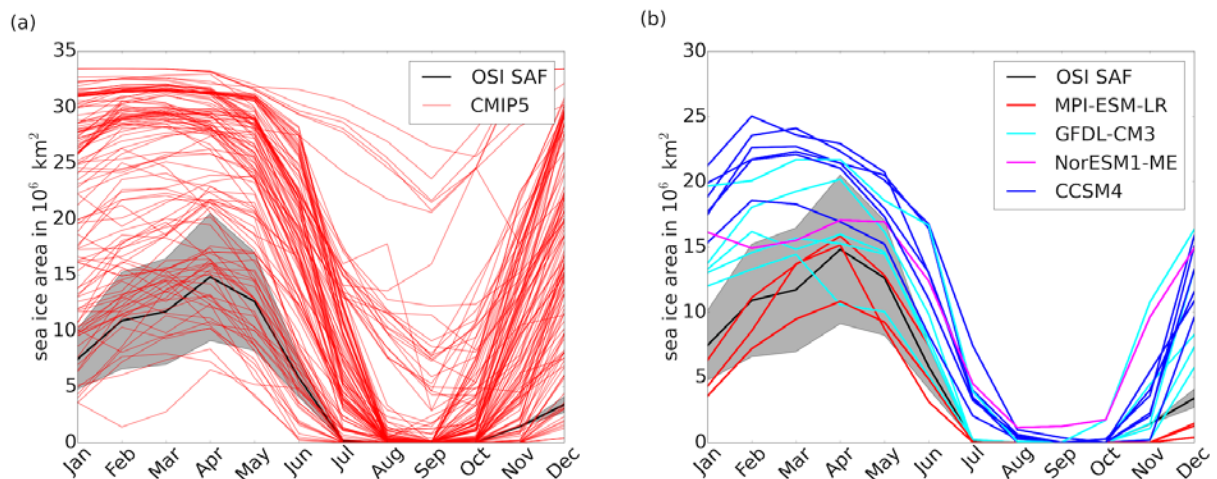


Figure 2: Area integrated sea-ice concentration mean seasonal cycle in the southern Barents Sea during 1979-2005: (a) individual ensemble simulation of CMIP5 models (red) in comparison with OSI SAF (black) mean (line) and standard deviation (grey shading); (b) four best models including MPI-ESM-LR (red) in comparison with OSI SAF (black) mean (line) and standard deviation (grey shading).

Assumptions

Being confronted with a set of more than 30 models providing very different projections of future climate in the Arctic, a quality based ranking of the ‘best’ models narrows down the range of results. The only way to evaluate the performance of the models is to compare their results with observations from the past, assuming that in this case the model is also of good quality simulating the future. We need atmospheric variables for the downscaling experiment. Since the atmosphere is strongly linked to the sea ice distribution, we assume that the atmospheric part of the chosen model is valid due to the evaluation of

the sea ice concentration. Furthermore, the climate change signal is carried via the atmospheric variables into the downscaling experiment.

rank	OSISAF 1979-2005 WP4.1 regions	normalized misfit	OSISAF 1979-2005 whole Arctic	normalized misfit	SSMI IFREMER 1992-2005 whole Arctic	normalized misfit
1	MPI-ESM-LR	1.00	MPI-ESM-LR	1.00	MPI-ESM-LR	1.00
2	MIROC4h	0.99	MPI-ESM-P	0.98	MPI-ESM-MR	0.95
3	MPI-ESM-MR	0.99	MPI-ESM-MR	0.98	CCSM4	0.95
4	GFDL-CM3	0.98	NorESM1-M	0.93	EC-EARTH	0.94
5	NorESM1-M	0.97	NorESM1-ME	0.89	MPI-ESM-P	0.94
6	MPI-ESM-P	0.96	CCSM4	0.88	CESM1-CAM-1FV2	0.94
7	ACCESS1-0	0.92	GFDL-CM3	0.85	NorESM1-ME	0.93
8	NorESM1-ME	0.88	IPSL-CM5A-MR	0.85	NorESM1-M	0.93
9	INMCM4	0.87	MIROC-ESM	0.84	GFDL-CM3	0.93
10	CCSM4	0.85	MIROC-ESM-CHEM	0.84	CNRM-CM5	0.91
11	HadGEM2-ES	0.84	MIROC4h	0.82	MIROC4h	0.90
12	MIROC-ESM	0.82	CESM1-CAM-1FV2	0.76	MIROC-ESM	0.88
13	EC-EARTH	0.80	ACCESS1-0	0.74	GFDL-ESM2M	0.88
14	MIROC-ESM-CHEM	0.72	GFDL-ESM2M	0.73	MIROC5	0.87
15	IPSL-CM5A-MR	0.72	CNRM-CM5	0.71	MIROC-ESM-CHEM	0.87
16	GFDL-ESM2M	0.71	IPSL-CM5A-LR	0.71	INMCM4	0.82
17	HadGEM2-CC	0.71	EC-EARTH	0.64	IPSL-CM5A-LR	0.81
18	CNRM-CM5	0.65	HadGEM2-CC	0.62	GFDL-ESM2G	0.81
19	HadGEM2-AO	0.61	FGOALS-s2	0.61	HadGEM2-CC	0.78
20	CESM1-CAM-1FV2	0.59	HadGEM2-ES	0.59	IPSL-CM5B-LR	0.77
21	HadCM3	0.51	MIROC5	0.57	ACCESS1-0	0.74
22	CanCM4	0.46	INMCM4	0.56	FGOALS-s2	0.71
23	CanESM2	0.46	IPSL-CM5B-LR	0.48	CSIRO-Mk3-6-0	0.70
24	FGOALS-s2	0.43	HadGEM2-AO	0.45	MRI-CGCM3	0.66
25	IPSL-CM5A-LR	0.42	GFDL-ESM2G	0.43	IPSL-CM5A-MR	0.66
26	GISS-E2-R	0.41	BCC-CSM1-1	0.36	BCC-CSM1-1	0.64
27	GISS-E2-H	0.40	CanCM4	0.29	FGOALS-g2	0.59
28	MIROC5	0.36	FGOALS-g2	0.28	GISS-E2-R	0.59
29	BCC-CSM1-1	0.33	CanESM2	0.22	HadGEM2-ES	0.51
30	GFDL-ESM2G	0.24	CSIRO-Mk3-6-0	0.15	HadCM3	0.48
31	IPSL-CM5B-LR	0.24	GISS-E2-R	0.12	CanCM4	0.43
32	FGOALS-g2	0.19	MRI-CGCM3	0.10	CanESM2	0.34
33	MRI-CGCM3	0.11	HadCM3	0.03	HadGEM2-AO	0.10
34	CSIRO-Mk3-6-0	0.00	GISS-E2-H	0.00	GISS-E2-H	0.00

Table 1: Ranking of CMIP5 models according to normalized misfit.

2.2. The MPI-ESM-LR and emission scenarios

For the downscaling experiments we picked the CMIP5 simulations of the Max Planck Institute for Meteorology's Earth System Model with a low resolution (MPI-ESM-LR). We apply the daily atmospheric variables surface air pressure, 2 m surface temperature and

specific humidity, 10 m wind, precipitation, and downward pointing long and short wave radiation at the surface from the historical run (1950-2005) and future (2006-2040) to the regional MITgcm. The future CMIP5 experiments are based on two different scenarios of potential greenhouse-gas concentrations in the atmosphere (leading to different radiative forcing for the atmosphere). These are the “representative concentration pathway” (RCP) emission scenarios [Moss *et al.*, 2010]. We choose to analyse two of those with an intermediate and a high concentration, respectively. By 2100 these scenarios reach a global change of radiative forcing relative to pre-industrial conditions of 4.5 and 8.5 W m⁻² (RCP4.5 and RCP8.5, respectively). ACCESS research focuses on the period 2010 to 2040 in which the change in radiative forcing reaches approximately 3 W m⁻² for the RCP 4.5 scenario and ~4 W m⁻² for the RCP 8.5 scenario.

The MPI-ESM-LR consists of the atmospheric model component ECHAM6 [Stevens *et al.*, 2013] and the ocean model MPIOM [Jungclauss *et al.*, 2013]. The sea-ice model is part of the MPIOM and consists of a thermodynamic-dynamic model based on a viscous-plastic rheology formulated by Hibler [1979]. The spatial resolution of the MPIOM consists of a bi-polar grid at a horizontal resolution of about 1.5° and 40 vertical levels. One pole is located over Greenland, which allows a resolution of about 20 km in the Fram Strait region [Notz *et al.*, 2013].

2.3. The MITgcm

We apply the atmospheric variables of the chosen model to a regional coupled ocean-sea ice set-up of the Massachusetts Institute of Technology General Circulation Model (MITgcm) [Marshall *et al.*, 1997].

The model domain covers the North Atlantic from approximately 50° N northward and the Arctic Ocean to the Bering Strait. The horizontal resolution consists of a 0.25° grid, which is rotated by 90° and shifted towards the equator, which passes through the model North Pole. Thus, the grid boxes are fairly equidistant with lengths ranging between 25.8 and 27.7 km. The ocean consists of 33 vertical levels, which are non-equidistantly spaced with depth ranging between 10 m close to the surface and 356 m at the maximum model depth of 4800 m.

Similar to the MPI-ESM-LR, the sea-ice model of the MITgcm consists of a thermodynamic-dynamic model based on a viscous-plastic rheology formulated by Hibler [1979]. See Castro-Morales *et al.* [2014] for a description of the set-up of the MITgcm in greater detail. Although the sea-ice models base on the same basic equations in both models, they differ considerably in the formulation of their parameterizations. One major advantage of the MITgcm is the ability to compute sub-grid scale ice and snow thickness. Castro-Morales *et al.* [2014] point out the sensitivity of the sub-grid snow and ice thickness distribution on the simulated mean ice thickness per grid box. A change from seven equally distributed sub-grid ice thickness categories (as suggested by Hibler [1984]) to 15 non-equally distributed ice categories, the distribution of which is based on observations, leads to an increase of around 1.5 m of ice thickness. This increase exceeds 2 m if the sub-grid snow thickness distribution has the same shape as the sub-grid ice distribution. The downscaling experiment thus uses 15 non-equally distributed ice categories and 15 equally distributed snow categories. The downscaling experiments (DEXP) are hereafter called DEXP-hist, DEXP-4.5 and DEXP-8.5 respectively to the emission scenario applied to it.

The MPI-ESM-LR CMIP5 simulations consist of three ensemble members each for the historical and the future scenarios. Each ensemble member is applied to the MITgcm for one of the DEXPs. The ensemble spread is a measure for the internal variability. The standard deviation of the individual members then serves as a measure of uncertainty due to internal variability.

3. Validation of the downscaling simulations

The sea ice thickness (sit) and concentration (sic) from the downscaling simulations as well as the original MPI-ESM-LR sea ice distributions are compared to satellite derived data and to results of the model PIOMAS, the Pan-Arctic Ice-Ocean Modeling and Assimilation System (PIOMAS) version 2.1 [Zhang and Rothrock, 2003]. The model simulation is based on an assimilation of satellite derived ice concentration data as well as sea surface temperature into a coupled sea ice-ocean model [Schweiger *et al.*, 2011]. PIOMAS covers the years 1980-2013. For the comparison we use sic data from OSI SAF, which covers the time period 1979-2009. In addition, Satellite derived sit will be taken from ten Ice, Cloud, and land Elevation Satellite (ICESat) campaigns for October-November and February-March (2007: March/April) during 2003-2008 with a grid resolution of 25 x 25 km [Kwok *et al.*, 2009].

Due to the sparseness data cover in that area we exclude the Canadian Arctic Archipelago (CAA) from this analysis.

3.1. Sea ice area: comparison with OSI SAF data and PIOMAS

Monthly mean sic is integrated Arctic wide to yield sea ice area (Fig. 3). DEXP-hist shows an ice area closer to the OSI SAF analysis than the MPI-ESM-LR. The DEXPs simulate about $1 \cdot 10^6 \text{ km}^2$ more ice area than the MPI-ESM-LR. The DEXP-hist ensemble mean is very similar to the 'observed' OSISAF sic. DEXP-hist is almost able to capture the full observed decreasing September sea ice area trend. The two future emission scenarios lead to very similar ensemble mean ice areas until 2020. After 2020, the ensemble mean ice area of RCP 8.5 is a couple of hundred thousand km^2 smaller than in the RCP 4.5 simulation of the DEXPs and MPI-ESM-LR. The largest differences occur in 2036 when the September ensemble mean ice area decreases by almost $1 \cdot 10^6 \text{ km}^2$ in DEXP-8.5. While the ensemble means do not show abrupt decreases of the September values such as observed in 2007 individual ensemble members for both RCP simulations exhibit such behaviour in several years. Note, that the aim of climate models is to reproduce the long-term, large-scale development of the climate as it results from external forcing (greenhouse gas releases, solar irradiation). The internal variability created by climate models may be similar to observations in a statistical sense, but they are not in phase with annual to multi-decadal variations of observed variables, if so its is by chance. The magnitude of the inter-annual variability and the trend of the September sic in the DEXP-hist are similar to those of OSI SAF. The DEXPs continue with a similar inter-annual variability and trend until 2040.

The PIOMAS simulation derives a September ice area offset of about $0.5 \cdot 10^6 \text{ km}^2$ larger than OSI SAF until 2006. Due to the data assimilation, PIOMAS is able to capture the sudden decrease in September 2007. The March sea ice area is very similar in OSI SAF and PIOMAS, $0.2\text{-}0.3 \cdot 10^6 \text{ km}^2$ larger than the DEXPs. Moreover, OSI SAF and PIOMAS show a larger inter-annual variability than the DEXPs and the MPI-ESM-LR. The decreasing trend in March is similar in all simulations and observations.

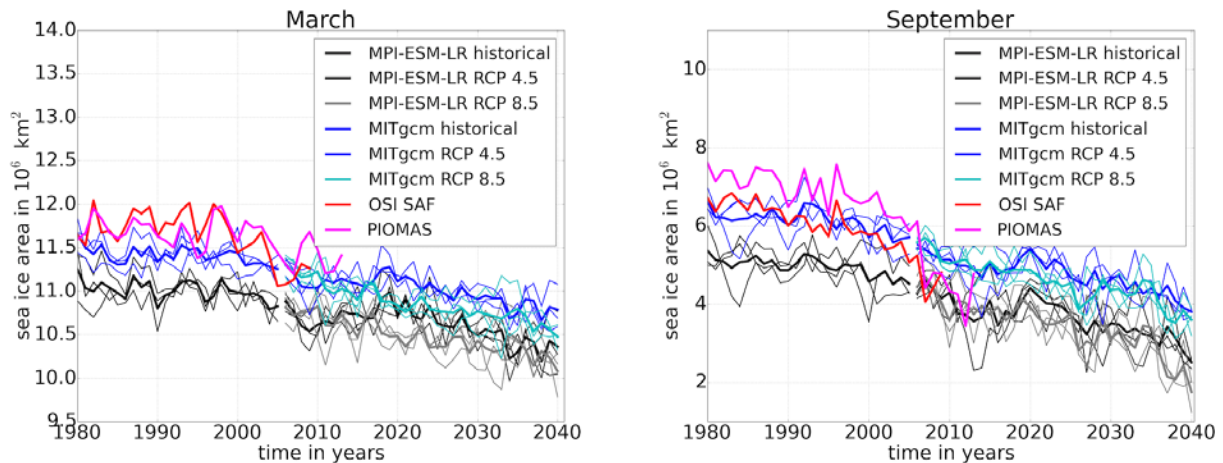


Figure 3: Arctic integrated sea ice area from the MPI-ESM-LR and the DEXPs for the time period 1980-2040. The RCP simulations start in 2006. Thick lines indicate the ensemble mean; thin lines show the individual ensemble member. OSI SAF sea ice area is shown in red and PIOMAS in magenta for comparison.

3.2. Sea ice volume: comparison with PIOMAS

The offset between the ensemble mean Arctic-wide sea ice volume by MPI-ESM-LR and DEXPs varies over time, in contrast to the offset in sea ice area, which is approximately constant. The September ice volume offset ranges between 3 and 4 10^3 km^3 during 1980-2005 with larger sea ice volume in DEXP-hist than in MPI-ESM-LR (Fig. 4). From 2006 on, the difference between these model experiments slowly decreases to 2 10^3 km^3 . The same difference in March ranges from 1.5 to 2 10^3 km^3 . For the future simulations the model experiments do not differ by more than 0.5 10^3 km^3 . The ensemble mean of the RCPs differ up to 0.5 10^3 km^3 , which is considerably less than the model spread of the individual ensemble members.

The magnitude of the sea ice volume simulated by PIOMAS is 2-4 10^3 km^3 larger than the ensemble mean of DEXP-hist as well as MPI-ESM-LR in March and September during 1980-1995. One ensemble member of the DEXP-hist exhibits similar magnitudes of ice volume. In the PIOMAS simulation the ice volume decreases rapidly since the early 1990s, with an absolute minimum in 2007. The same strong decline does not show in the ensemble means of MPI-ESM-LR and DEXPs. However, individual DEXP ensemble members of both the historical and the RCP simulations show a strong negative trend as seen in the PIOMAS simulation, as well as strong decline events such as the one shown by PIOMAS for 2007.

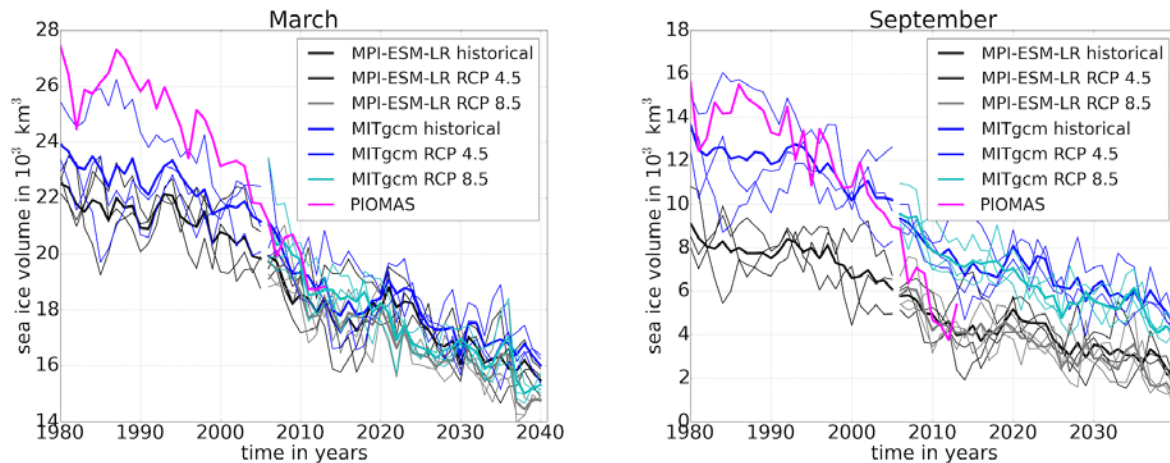


Figure 4: Arctic integrated sea ice volume from the MPI-ESM-LR and the DEXPs for the time period 1980-2040. The RCP simulations start in 2006. Thick lines indicate the ensemble mean; thin lines show the individual ensemble member. PIOMAS sea ice volume is shown in magenta for comparison.

3.3. Sea ice thickness: comparison with ICESat and PIOMAS

Figure 5 shows the mean of the months October, November for 2003-2007 and the means of February-April for 2004-2008 as derived from ICESat and as simulated by the models. The PIOMAS ice thickness is closer to ICESat than the other simulations. All models show too thin ice north of Greenland and the CAA. In addition, thicker ice (ice > 2 m) can be found in parts of the Central Arctic and along Beaufort and Chuckchi Sea coastline in ICESat and PIOMAS in winter, which is absent in the DEXPs and the MPI-ESM-LR. The observed ice thickness based on ICESat ranges between 1.5 and 2.5 m in the Central Arctic. Both, the ensemble means of MPI-ESM-LR and DEXP-8.5 show about 1.5 m of ice in this area. Moreover, the ice is also too thin along the Siberian coastline by about 0.5 m. The model spread in the DEXP-8.5, indicated by the ensemble standard deviation, is largest along the entire Arctic coastline and ranges from 0.3 to 0.5 m. The very thick multi year ice is also underrepresented in the ensemble mean over the months February-March (2007: March-April) for the years 2004-2008 (Fig. 5a). However, the ice is similarly thick, around 2.5 m in the Central Arctic in PIOMAS, the MPI-ESM-LR and DEXP-8.5 in comparison with ICESat. In contrast to the summer season, the ensemble mean ice is too thick in the Laptev Sea by approximately 1 m and too thin by about 0.5 m north of the Bering Strait and along the Canadian coastline. The ensemble spread ranges mostly between 0.2 and 0.3 m over the entire Arctic in DEXP-8.5. The comparison of simulated ice thickness with those derived from the ICESat satellite confirms the indication gained from the ice volume comparison: the ice is generally too thin in MPI-ESM-LR and DEXP in the ensemble means as well as in all individual members.

Hardly any differences are seen between the different RCP simulations neither in winter nor in summer. Although the differences between the ensemble means of the DEXP-4.5 and DEXP-8.5 simulations are mostly small, the DEXP-8.5 ensemble mean is closer to observations and PIOMAS.

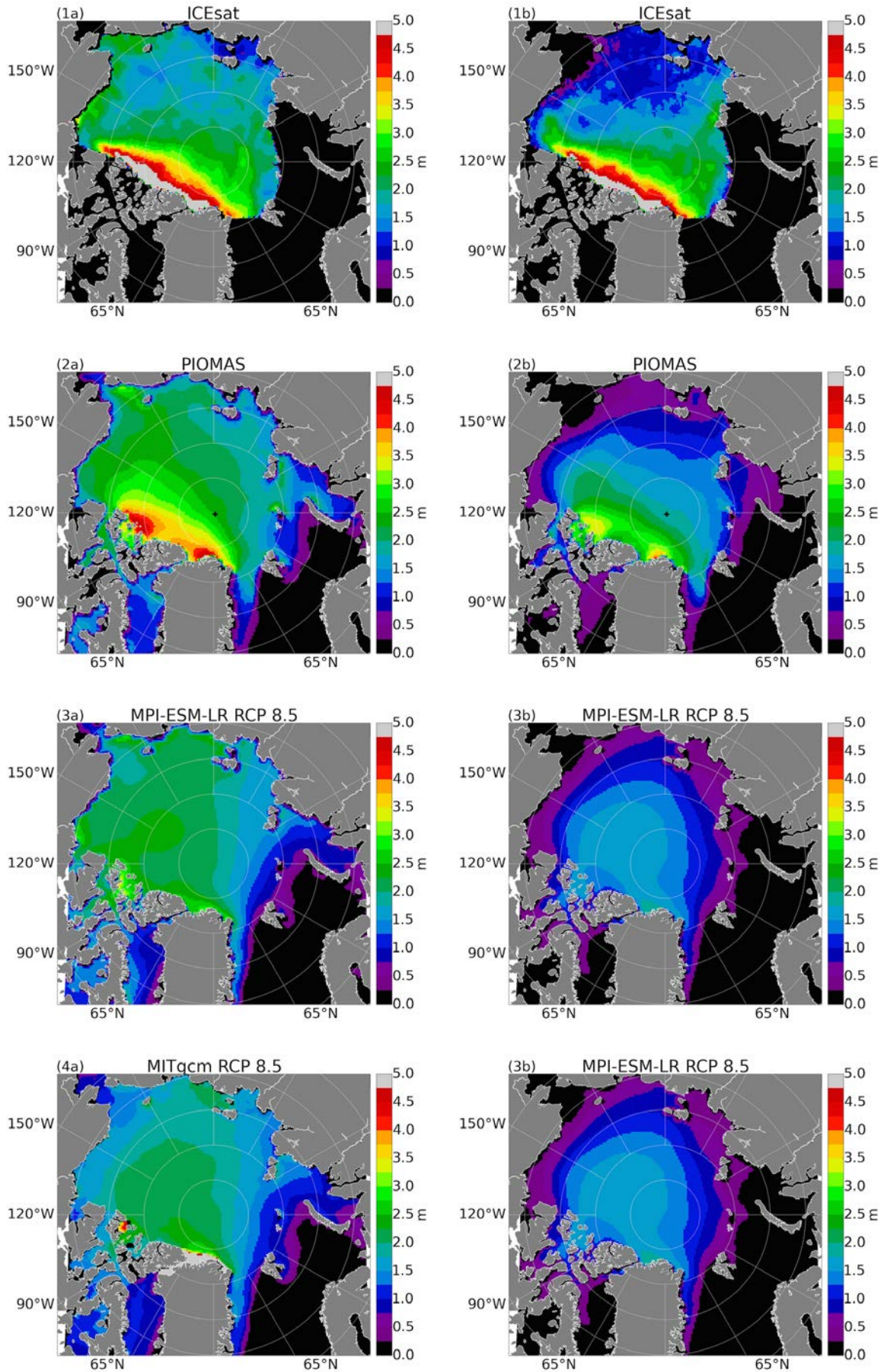


Figure 5: Mean ice thickness for (a) February-April 2004-2008 and (b) October and November 2003-2007. (1) ICESat is compared to (2) PIOMAS and the ensemble mean of (3) MPI-ESM-LR and (4) DEXP-8.5.

4. Development of Arctic sea ice until 2040 – the downscaling results

For all sea ice properties projected by the downscaling experiments, differences between the DEXP-4.5 and DEXP-8.5 are small. For the DEXP-8.5, however, we find declining sea ice area and volume trends closer to observations for the available period 2006 to 2013. Therefore, the following discussion focuses on the DEXP-8.5 simulations only.

As a measure for the projected change of sea ice conditions monthly mean values of the last 15 years of the DEXP-hist from 1991-2005 are compared to the last 15 years of the DEXP-8.5 2026-2040. Furthermore, we determine the number of days per month (per year, respectively) for which sic and sit meet specific thresholds: sic \leq 20 %, 40 % and 60 % and sit \leq 0.5 m, 1.0 m and 1.5 m respectively.

4.1. Development of sic and sit in March and September

Figure 6 addresses the change of ensemble mean sic in September and March from 1991-2005 to 2026-2040. The ensemble mean sic in September decreases almost in the entire Arctic by at least 10 %. The largest decrease of up to 70 % occurs along the Nordic Seas ice edge in September and March. The ensemble spread ranges from 5 to 10 % in a large area in the Chukchi Sea and parts of the Beaufort Sea, whereas the largest ensemble spread occurs as well along the Nordic Seas ice edge with a magnitude of up to 20 % in September. The red line in Fig. 6 indicates the 15 % contour line for the ensemble mean for the years 2026-2040. The green line visualizes the 15 % contour line for the ensemble mean of the earlier time period 1991-2005. In September, the 15 % sic contour retreats considerably further north in the Barents and Kara Sea from the earlier to the later time period. In contrast, the red 15 % contour is still reaching the coast in parts of the Laptev and the East Siberian Sea. Furthermore, the red 15 % contour line retreats in the Beaufort Sea leaving a corridor of below 15 % sea ice along the Canadian coast in September.

In March, a reduction of the sea ice concentration is only projected for the Nordic Seas and the Barents Sea. The ensemble mean ice edge retreats between about 50 km in the east Greenland Sea to 200 km in the northern Barents Sea. There, sic decreases up to 70 % with an ensemble spread up to 20 %.

The change of monthly mean sit between the two periods is shown in Figure 7. In contrast to the changes in sic, the largest decreases of the ensemble mean sit occur north of Greenland with more than 2 m of change whereas in the central Arctic sit decreases by about 1 m with an ensemble spread of 0.1-0.2 m. The red line indicates the 0.5 m contour line of the ensemble mean for 2026-2040. In the vicinity to the Arctic coastlines all sea ice is projected to be thinner than 0.5 m for 2026-2040, in contrast to 1991-2005 (0.5 m contour line is indicated by the green line). The red 0.5 m contour line retreats to 80° N north of Svalbard, where the ensemble spread ranges between 0.1 and 0.2 m.

Although the sit decreases in almost the entire Arctic by at least 0.25 m in March, the 0.5 m contour line retreats further north only along the Nordic sea ice edge. The retreat is of a similar magnitude as in the sic retreat which ranges from about 50 km in the east Greenland Sea to 200 km in the northern Barents Sea. The ice thickness decreases

between 0.5 and 1 m in the central Arctic in March with an ensemble spread of about 0.2 - 0.3 m.

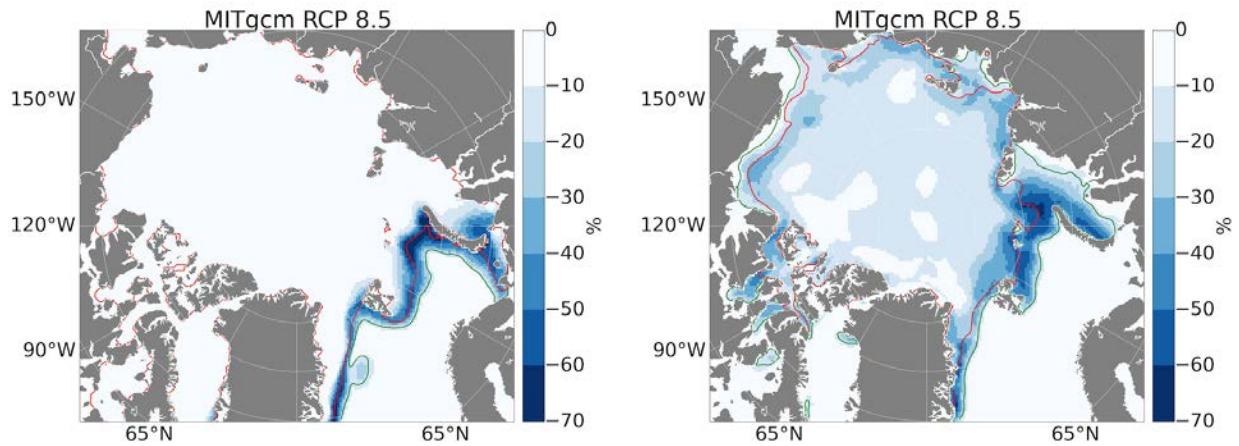


Figure 6: Decrease of ensemble mean sic is shown from mean(1991-2005) to mean(2026-2040). The mean change is shown for March (left) and September (right) of DEXP-8.5. The green line indicates the 15 % contour line of the mean(1991-2005), the red line shows the 15 % contour line of the mean(2026-2040).

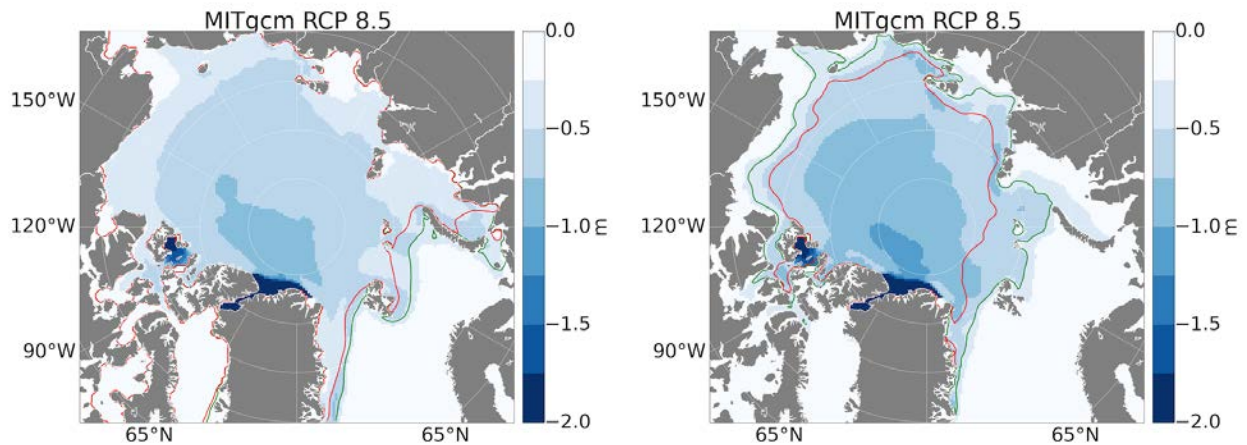


Figure 7: Decrease of ensemble mean sit is shown from mean(1991-2005) to mean(2026-2040). The mean change is shown for March (left) and September (right) of DEXP-8.5. The green line indicates the 0.5 m contour line of the mean(1991-2005), the red line shows the 0.5 m contour line of the mean(2026-2040).

4.2. Development of 'low ice condition' days

We are interested in how the ship traffic might change in the decades ahead due to changes in sea ice cover along the Northern Sea Routes (NSR). We assume that ship traffic will increase if the sea ice along the NSR is navigatable for ships. Different types of ships are able to navigate through different conditions of sic and sit. Therefore, we analyse daily mean sic and sit of DEXP-8.5 with respect to the number of days for which sic and sit fall below specific thresholds. Since model output with a daily frequency is available only after 2006, the changes of the years 2026-2040 are compared to the time period 2006-2020. The thresholds chosen are $sic \leq 20, 40$ and 60% and $sit \leq 0.5, 1.0$ and 1.5 m. These thresholds base on the personnel communication with Nils Reimer

from the Hamburgische Schiffbau-Versuchsanstalt (HSVA), a work package 2 partner in ACCESS.

We compare ensemble means of sic with 'low ice conditions' for the years 2006-2020 and 2026-2040 in Fig. 8. In the earlier period most parts of the Barents and Kara Sea have $\text{sic} \leq 20\%$ for more than 90 days per year including the Kara Strait (strait between the Barents Sea and the Kara Sea). The Vilkitsky Strait (the strait connects the Kara Sea with the Laptev Sea) and the Dmitry Laptev Strait (Strait between the Laptev and the east Siberian Sea) are open ($\text{sic} \leq 20\%$) for at least 70 days, while large parts of the Laptev Sea, the East Siberian Sea and the De Long Strait (Strait between East Siberian Sea and the Chukchi Sea) have $\text{sic} \leq 60\%$ for no longer than 60 days, $\text{sic} \leq 40\%$ for 50 days and only 30 days for $\text{sic} \leq 20\%$. $\text{Sic} \leq 20\%$ occurs more than 90 days during an average year 2006-2020 along the coast in the Beaufort Sea in the time period. The three ensemble members exhibit a spread up to 15 days along the ice edge in the entire Arctic. The number of days with 'low ice conditions' increases in the area adjacent to the Arctic coastline in the later time period. For more than 90 days $\text{sic} \leq 40\%$ along the entire coastline, with the exception of some parts in the Laptev and East Siberian Sea where $\text{sic} \leq 20\%$ occurs between 50 and 70 days.

The ensemble means of sit with 'low ice conditions' are shown in Fig. 9 for 2006-2020 and 2026-2040. A narrow strip of coastal area (~ 50 km) shows $\text{sit} \leq 0.5$ m for about 90 days during the earlier time period. This area widens considerably if we use the threshold of $\text{sit} \leq 1.0$. Moreover, only a small area is thicker as 1.5 m throughout the entire year. The number of days with 'low ice conditions' increases during the later period 2026-2040. The ensemble spread increases to 15 days in most coastal areas for $\text{sit} \leq 0.5$ m and up to 30 days in many regions within the entire Arctic.

Since the various straits along the Russian coast are very narrow, ice might get stuck there and block the strait. However, figure 8 and 9 show that ice is accumulating east of some straits especially east of the Dmitry Laptev Strait. DEXP-8.5 indicates that the straits are open ($\text{sic} \leq 20\%$) for more than 80 days (plus minus 15 days of model spread) per year during an average year. The coastline along the Laptev and East Siberian Sea is open for considerable fewer days. Note, that this analysis does not indicate whether the straits are open at the same time.

Be reminded that the validation showed that sit in the DEXPs is too thin in the central Arctic as well as along the coastal regions. Therefore, caution is needed during the analysis of future sit distributions.

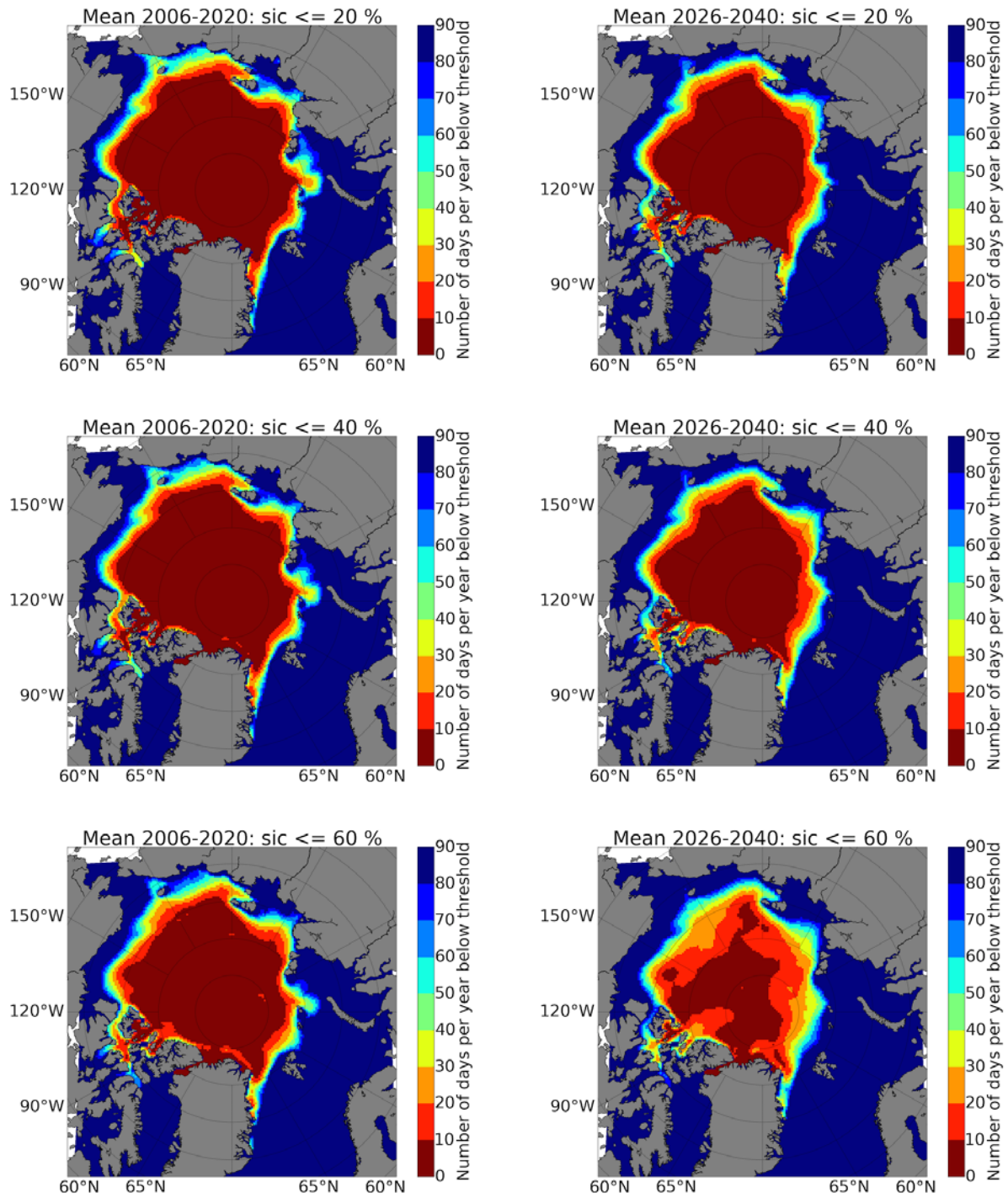


Figure 8: Ensemble mean of number of 'low ice condition' days per year with sic ≤ 20, 40 and 60 %, respectively, for the mean from 2006-2020 and 2026-2040, respectively. All results from DEXP-8.5.

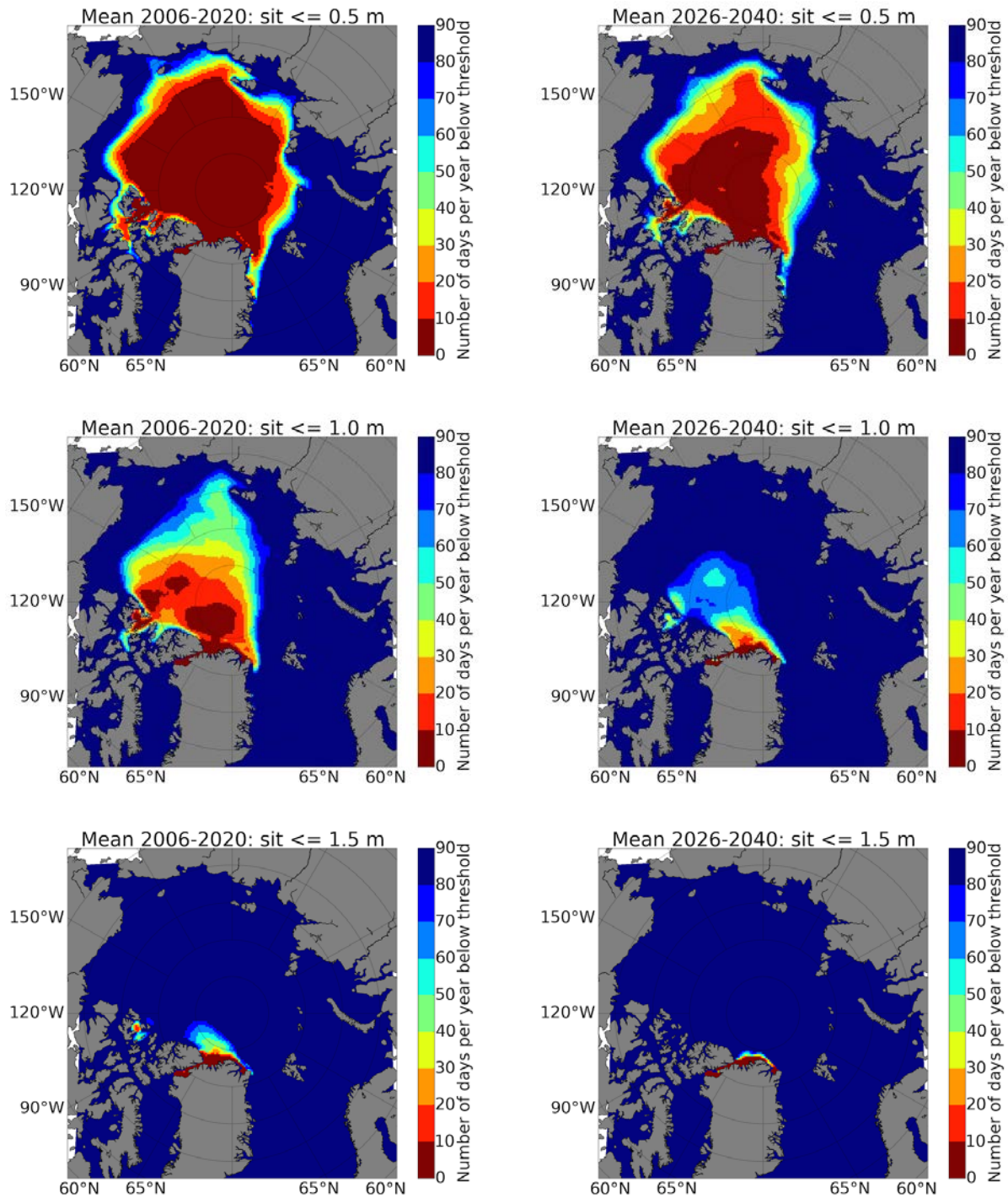


Figure 9: Ensemble mean of number of 'low ice condition' days per year with $\text{sit} \leq 0.5$, 1.0 and 1.5 m, respectively, for the mean from 2006-2020 and 2026-2040, respectively. All results from DEXP-8.5.

4.3. Changes along a Northeast Passage

The previous section described the mean change of 'low ice condition days'. For navigational purposes 'low-ice' conditions along a passage from A to B are more relevant. To exemplify the possibilities of evaluating the change of sea ice conditions relevant for shipping, we chose one possible route of a Northeast Passage (NEP) and calculate the number of days on which all grid boxes along this route are below a certain sic or sit. The location of the passage is very similar to those suggested by HSVA in their ACCESS

report D2.16 figure 6 route option 1. It differs only in the chosen passage through the New Siberian Islands.

This analysis computes the number of days where the whole route consists of ‘low ice conditions’. Note, that a ship will not be able to navigate along the complete NEP within one day. Moreover, if a ship encounters a region with ‘high ice conditions’, it might be able to navigate along an alternative route. This option is not included in this analysis. Therefore, the total number of days per month with ‘low ice conditions’ is small compared to the previous subchapter, since all grid boxes along the route have to meet the threshold criteria at the same day to be counted. The chosen route goes through many straits, which may be blocked by ice. However, the downscaling simulation shows that ice blocks the route east of the Vilkitsky Strait and/or east of the Dmitry Laptev Strait, while the straits themselves are mostly open.

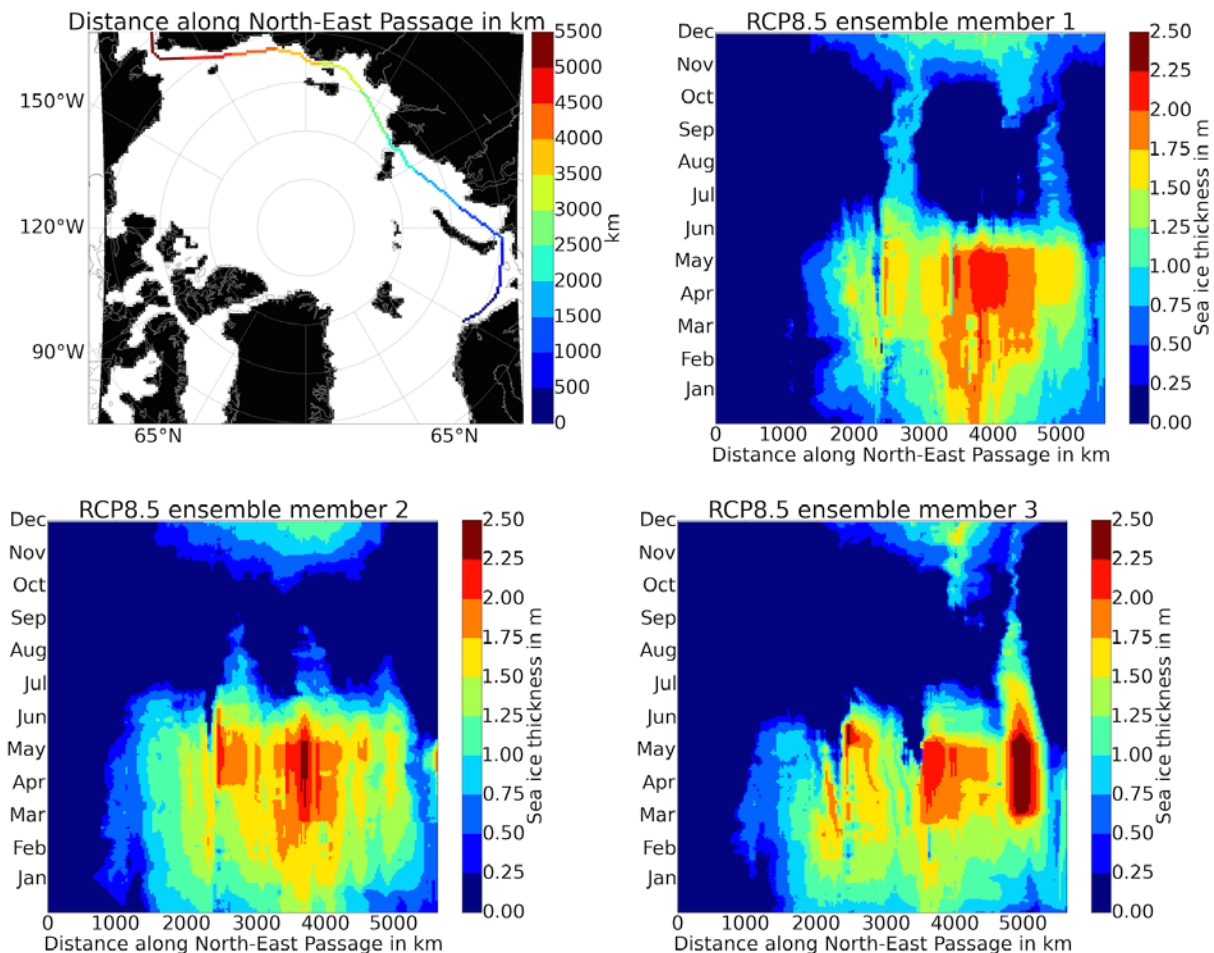


Figure 10: Position of a Northeast Passage (upper left) and daily sea ice thickness distributions along the Northeast Passage during 2040 for individual ensemble members. All results are from DEXP-8.5.

Figure 10 shows the daily sea ice thickness along the NEP for each ensemble member in the year 2040 of DEXP-8.5. It gives an impression not only of the ensemble spread, but also shows that over extended periods in summer it is only at specific positions that a complete ice-free status of the passage is prevented. These are the aforementioned areas east of the islands. The ensemble mean and standard deviation of the number of days with sic and sit being below a threshold along the NEP of the time periods 2006-2020 and 2026-2040 are shown in figure 11. The mean number of days with ‘low ice conditions’ as well as the ensemble spread increase considerably for the later time

period. The 'low ice' period starts one month earlier and ends one month later in the later time period. Moreover, the length of the period with $\text{sit} \leq 1.5 \text{ m}$ elongates by four months, lasting from May to February.

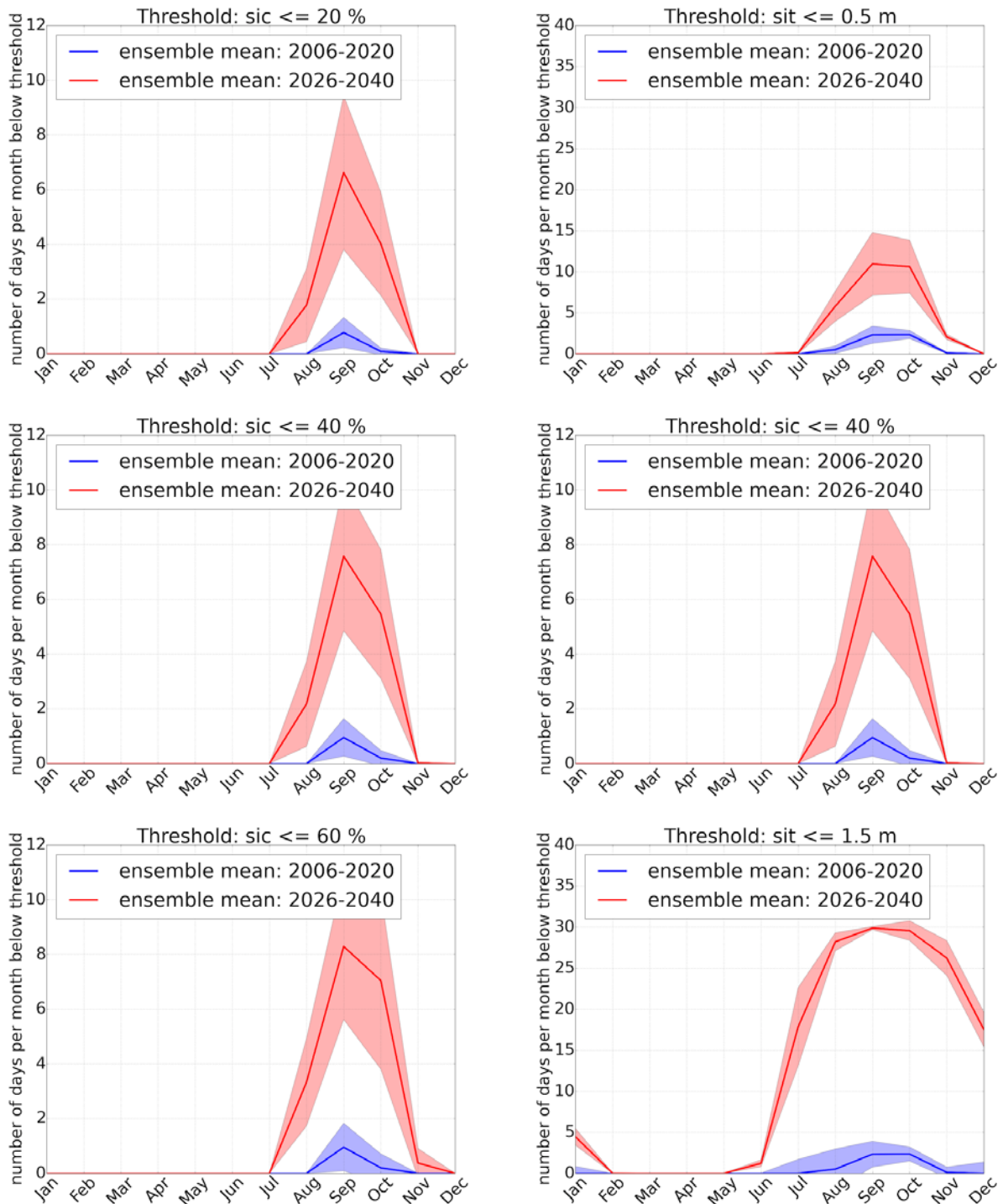


Figure 11: Ensemble mean (line) and standard deviation (shaded area) of number of days per month with sic (left) and sit (right) below thresholds along the NEP. All results from DEXP-8.5 .

5. Summary and Conclusions

In the framework of the ACCESS project we analysed the performance of CMIP5 models with regard to their skill to simulate 20th century sea ice concentration as observed. The

mean seasonal cycle of sic is compared to two different Satellite derived products for each grid box of a common 0.25° grid over two different time periods. The ranking of individual CMIP5 models according to performance depends on the area of comparison and the Satellite product used for comparison. Only MPI-ESM-LR has a sic closest to the observations in all conducted analyses. This results is in agreement with previous studies of CMIP5 sea ice analyses, e.g. by *Massonnet et al.* [2012] and *Wang and Overland* [2012], who also listed the MPI-ESM-LR among the better models. We thus pick MPI-ESM-LR as a source for model forcing to be applied in downscaling experiments where its atmospheric variables force a coupled Arctic sea-ice ocean model. This is done to perform projections for future sea ice development with a higher spatial resolution.

The comparison of the original MPI-ESM-LR and the downscaled simulation with Satellite derived sic and sit shows that the downscaled simulation produces more and thicker ice than the MPI-ESM-LR and is closer to satellite observations than the CMIP5 model. In particular, the magnitude, trend and inter-annual variability of the ensemble mean September sic is very similar to observed sic from OSI SAF for the historical simulation (1979-2005). Abrupt decreases of sic as observed in 2007 occur in the ensemble mean of downscaled simulation for the RCP-8.5 experiment. As expected for a forcing from a fully coupled climate model, however, the timing of single events attributed to internal variability, as for example the 2007 sea ice minimum, are not simulated with the exact timing as observed.

Although the downscaled simulations show a generally thicker sea ice than the original MPI-ESM-LR simulations, these are thinner than observed in the available period of ICESat satellite data analysis. Therefore, caution is needed in interpretation of the projected future sit development. The situation is somewhat different if using single ensemble members instead of an ensemble mean. One ensemble member of the downscaled historical simulation has similar sea ice volume, inter-annual variability and trend as the assimilated PIOMAS simulation during March and September. Moreover, only individual ensemble simulations were able to reproduce abrupt decreases in sea ice volume of similar magnitude as observed. Since the sudden changes occur in different years, the ensemble mean does not show these. Although the differences between the ensemble means of the DEXP4.5 and DEXP-8.5 simulations are mostly small until 2040, the DEXP-8.5 ensemble mean is closer to observations and PIOMAS. Note, that PIOMAS is also a model and cannot be used as observations for validation purposes. However, since PIOMAS assimilates observations its skill is high in simulating sea-ice (see section 3.3). Therefore, it is used as a first reference if no observations are available.

During the period 2026-2040, the ensemble mean September sic decreases almost in the entire Arctic by at least 10 % with an ensemble spread of 5 to 10 %. The largest decrease of up 70 % occurs along the Nordic Seas sea ice edge in September and March (ensemble spread up to 20 %). Despite a general shrinking of sea ice cover, the 15 % sic contour still reaches the coast in parts of the Laptev and the East Siberian Sea in the September ensemble means. In the Amerasian part of the Arctic the 15 % contour line retreats north in the Beaufort Sea leaving a path along the Canadian coast in September. In March, the sea ice concentration retreats only in the Nordic Seas along the ice edge in our model domain. The ice thickness decreases around 1 m with an ensemble spread of 0.1-0.2 m in the central Arctic. All sea ice is going to be thinner than 0.5 m along the Arctic coastlines during the mean of 2026-2040, which was not the case

along the Siberian coast during the mean of 1991-2005. The 0.5 m contour line retreats to 80° N north of Svalbard, where the ensemble spread ranges between 0.1 and 0.2 m. In March, the 0.5 m contour line retreats further north only along the Nordic sea ice edge. Its northward retreat ranges from about 50 km in the east Greenland Sea to 200 km in the northern Barents Sea.

Throughout the year, sic \leq 40 % for more than 90 days along the entire coastline; with the exception of some parts of the Laptev and the East Siberian Sea where sic \leq 20 % occurs between 50 and 70 days. A wide strip of coastal area consists of sit \leq 0.5 m for about 90 days until 2040. This area considerably widens if sit \leq 1.0 is taken as a threshold and only a small area is thicker as 1.5 m throughout the entire year. A near-coastal variety of the NEP passes many narrow straits. The downscaling experiments show that ice blocks the route east of the Vilkitsky Strait and/or east of the Dmitry Laptev Strait, while the straits themselves are mostly open. The DEXP-4.5 and DEXP-8.5 indicate that the straits are open (sic \leq 20 %) for more than 80 days (with 15 days of model spread) per year during an average year of the time period 2026-2040. The analysis of sic and sit along one of the possible Northeast Passages for the time periods 2006-2020 and 2026-2040 shows that the mean number of days where sic and sit along the entire NEP are under 'low ice' conditions' as well as the ensemble spread increases considerably during the later time period. Moreover, the length of 'low ice condition' periods elongates by at least two months. This period starts one month earlier and ends on month later. The ice thins so much, that the period with at least one day of sit \leq 1.5 m along the NEP lasts eight months from May to February during 2026-2040.

References:

Castro-Morales, K., F. Kauker, M. Losch, S. Hendricks, K. Riemann-Campe, and R. Gerdes (2014), Sensitivity of simulated Arctic sea ice to realistic ice thickness distributions and snow parameterizations, *J Geophys Res-Oceans*, 119(1), 559-571, doi:10.1002/2013jc009342.

Gautier, D. L., et al. (2009), Assessment of Undiscovered Oil and Gas in the Arctic, *Science*, 324(5931), 1175-1179, doi:10.1126/Science.1169467.

Hibler, W. (1979), A dynamic thermodynamic sea ice model, *Journal of Physical Oceanography*, 9(4), 815-846, doi:10.1175/1520-0485(1979)009<0815:ADTSIM>2.0.CO;2.

Hibler, W. (1984), The role of sea ice dynamics in modeling CO₂ increases, *Climate processes and climate sensitivity*, 238-253, doi:10.1175/1520-0485(1979)009<0815:ADTSIM>2.0.CO;2.

Jungclaus, J. H., N. Fischer, H. Haak, K. Lohmann, J. Marotzke, D. Matei, U. Mikolajewicz, D. Notz, and J. S. von Storch (2013), Characteristics of the ocean simulations in the Max Planck Institute Ocean Model (MPIOM) the ocean component of the MPI-Earth system model, *J Adv Model Earth Sy*, 5(2), 422-446, doi:10.1002/Jame.20023.

Kwok, R., G. F. Cunningham, M. Wensnahan, I. Rigor, H. J. Zwally, and D. Yi (2009), Thinning and volume loss of the Arctic Ocean sea ice cover: 2003-2008, *J Geophys Res-Oceans*, 114, C07005, doi:10.1029/2009jc005312.

- Marshall, J., A. Adcroft, C. Hill, L. Perelman, and C. Heisey (1997), A finite-volume, incompressible Navier Stokes model for studies of the ocean on parallel computers, *J Geophys Res-Oceans*, 102(C3), 5753-5766, doi:10.1029/96jc02775.
- Massonnet, F., T. Fichefet, H. Goosse, C. M. Bitz, G. Philippon-Berthier, M. M. Holland, and P. Y. Barriat (2012), Constraining projections of summer Arctic sea ice, *The Cryosphere*, 6(6), 1383-1394, doi:10.5194/tc-6-1383-2012.
- Moss, R. H., et al. (2010), The next generation of scenarios for climate change research and assessment, *Nature*, 463(7282), 747-756, doi:10.1038/Nature08823.
- Notz, D., F. A. Haumann, H. Haak, J. H. Jungclaus, and J. Marotzke (2013), Arctic sea-ice evolution as modeled by Max Planck Institute for Meteorology's Earth system model, *J Adv Model Earth Sy*, 5(2), 173-194, doi:10.1002/Jame.20016.
- Schweiger, A., R. Lindsay, J. L. Zhang, M. Steele, H. Stern, and R. Kwok (2011), Uncertainty in modeled Arctic sea ice volume, *J Geophys Res-Oceans*, 116, C00D06, doi:10.1029/2011jc007084.
- Stevens, B., et al. (2013), Atmospheric component of the MPI-M Earth System Model: ECHAM6, *J Adv Model Earth Sy*, 5(2), 146-172, doi:10.1002/Jame.20015.
- Stroeve, J. C., V. Kattsov, A. Barrett, M. Serreze, T. Pavlova, M. Holland, and W. N. Meier (2012), Trends in Arctic sea ice extent from CMIP5, CMIP3 and observations, *Geophys Res Lett*, 39, L16502, doi:10.1029/2012gl052676.
- Taylor, K. E., R. J. Stouffer, and G. A. Meehl (2012), An Overview of Cmp5 and the Experiment Design, *B Am Meteorol Soc*, 93(4), 485-498, doi:10.1175/Bams-D-11-00094.1.
- Wang, M. Y., and J. E. Overland (2012), A sea ice free summer Arctic within 30 years: An update from CMIP5 models, *Geophys Res Lett*, 39, L18501, doi:10.1029/2012gl052868.
- Zhang, J. L., and D. A. Rothrock (2003), Modeling global sea ice with a thickness and enthalpy distribution model in generalized curvilinear coordinates, *Mon Weather Rev*, 131(5), 845-861, doi:10.1175/1520-0493(2003)131<0845:Mgsiwa>2.0.Co;2.